Ann. Geophys. Discuss., https://doi.org/10.5194/angeo-2018-66
Manuscript under review for journal Ann. Geophys.
Discussion started: 3 July 2018

Annales Geophysicae Discussions
Open Access
EGU

Statistical Analysis of Magnetopause Crossings at Lunar Distances

Johannes Z. D. Mieth[1], Dennis Frühauff[1], and Karl-Heinz Glassmeier[1]

[1]Technische Universität Braunschweig, Institut für Geophysik und extraterrestrische Physik, Mendelsohnstraße 3, 38106 Braunschweig, Germany

Correspondence: Johannes Z. D. Mieth (j.mieth@tu-braunschweig.de)

Abstract. Different magnetopause models with a diverse level of complexity are in use. They have in common to be mainly based on near-earth observations, i.e., they use measurements at distances of about ± 10 Earth radii. Only very few observations of magnetopause crossings at larger distances are used for model fitting. In this study we compare position and direction predictions of the Shue et al. (1997) magnetopause model with actual observations of magnetopause crossings identified using the ARTEMIS spacecraft at lunar distance, about 60 Earth radii. We find very good agreement between prediction and observation for the magnetopause position. Also the magnetopause normal directions are reasonably well predicted.

1 Introduction

The magnetopause plays an important role for space weather processes as it is the primary interaction zone between the solar wind plasma and the Earth's magnetosphere. The magnetopause is defined as the plane where the solar wind pressure is balanced by the Earth's magnetic field pressure (e.g. Glassmeier et al., 2008). In 1997 Shue and co-workers presented a very advanced model to predict the magnetopause (MP) position and its normal direction under different solar wind (SW) conditions (Shue et al., 1997). Using data of magnetopause crossings of the ISEE 1 and 2, AMPTE/IRM, and IMP 8 satellites they modelled the magnetopause radial distance r with the functional form $r = r_0 \left[2/\left(1+\cos\theta\right)\right]^{\alpha}$. Here r_0, θ, and α denote the standoff distance, the angle between the Sun-Earth line and the direction of r, and the magnetopause flaring parameter, respectively (Fig.3). Shue et al. (1997) found this form to be only depended on the B_z component of the interplanetary magnetic field (IMF) and the solar wind dynamic pressure D_p. This functional model is mathematical axially symmetric around the x-axis in geocentric solar ecliptic (GSE) and geocentric solar magnetospheric (GSM) coordinates (Hapgood, 1992). Measurements used for the determination of the fitting parameters are mainly from distances of ± 10 Earth radii (R_E) on the x-axis with only a few data points expanding up to about $30\,\mathrm{R_E}$ downtail. As detailed the Shue model is, it requires further observations from higher latitudes as well as crossings further downtail from the Earth to provide a more realistic 3D magnetopause model (Shue and Song, 2002). Extensions of the Shue model were thus presented by, e.g., Lin et al. (2010) and Wang et al. (2013). However, all the proposed models are still characterized by using only a very limited number of measurements at greater distances downtail. This is where our study contributes. By using plasma and magnetic field measurements from the ARTEMIS mission we validate the Shue model at radial distances of about $60\,\mathrm{R_E}$ downtail.

Ann. Geophys. Discuss., https://doi.org/10.5194/angeo-2018-66
Manuscript under review for journal Ann. Geophys.
Discussion started: 3 July 2018

Annales Geophysicae Discussions
Open Access
EGU

2 Data selection and analysis procedure

The *Acceleration, Reconnection, Turbulence, and Electrodynamics of the Moon's Interaction with the Sun* (ARTEMIS) Mission (Angelopoulos, 2010) provides long term measurements of the plasma environment in the terrestrial magnetosphere at lunar distances, about $60\,\mathrm{R_E}$. Since 2011 the two spacecraft THB and THC orbit the Moon and provide excellent measurements of the plasma environment there. The THB and THC spacecraft originate from the THEMIS mission (Angelopoulos, 2008), a NASA Medium-Class Explorers (MIDEX) mission, launched on February 17, 2007 and designed to investigate the trigger mechanisms and evolution of magnetospheric substorms. Five identical spacecraft were put into Earth's orbit to line up along the magnetotail. After the primary mission phase the two outermost spacecraft were lifted into a lunar orbit. Since May 2011 both probes are in stable equatorial and eccentrical orbits.

2.1 Observations

Our study covers a time span of five years, starting January 2011 and lasting until December 2015. Different types of data products are used to determine magnetopause position and direction. The electrostatic analyzer (ESA) (McFadden et al., 2008) provides ion and electron flux density over a broad energy band from only a few eV up to $30\,\mathrm{keV}$. We use time resolved ion energy data with a resolution of about $3\,\mathrm{s}$ in this study. In order to generate this data set, measurements with higher temporal resolution are integrated over a spin period of the spacecraft. The plasma data are complemented by measurements from the ARTEMIS fluxgate magnetometer (FGM) (Auster et al., 2008), providing vector magnetic field data which we average over the spin period of about 3 s.

2.2 Data processing

The spacecraft position vector as well as the measured magnetic field vector are first represented in the GSE coordinate system and corrected by a mean solar wind aberration angle $\alpha = \tan^{-1}(v_\mathrm{E}/v_\mathrm{SW})$, with $v_\mathrm{E} = 30\,\mathrm{kms^{-1}}$, the velocity of the Earth around the Sun and $v_\mathrm{SW} = 400\,\mathrm{kms^{-1}}$, a commonly used value for the mean solar wind speed (Hansen et al., 2007). The aberration corrected data are subsequently transformed into GSM coordinates. Unless otherwise indicated GSM coordinates are always aberration corrected in the following.

To determine the MP normal direction, minimum variance analysis (MVA) (e.g., Paschmann and Daly, 1998) is applied to the magnetic field data within five minutes before and after any identified MP crossing, which will be defined below. As the MVA analysis only provides the orientation but not the direction of the normal, we assume the magnetopause normal to be always directed outwards of the MP, into the direction of the magnetosheath.

To calculate model predictions of MP positions, SW observations are needed as input parameters to the Shue model. We use 1-minute solar wind magnetic field and plasma data as extracted from NASA/GSFC's OMNI data set through OMNIWeb. This dataset contains information on the plasma parameters at the bowshock's nose. To take into account the time delay between bowshock's nose observations and conditions at the actual MP position 1-hour mean averages of solar wind parameters are used to determine the model values of the MP position and normal direction.

Ann. Geophys. Discuss., https://doi.org/10.5194/angeo-2018-66
Manuscript under review for journal Ann. Geophys.
Discussion started: 3 July 2018

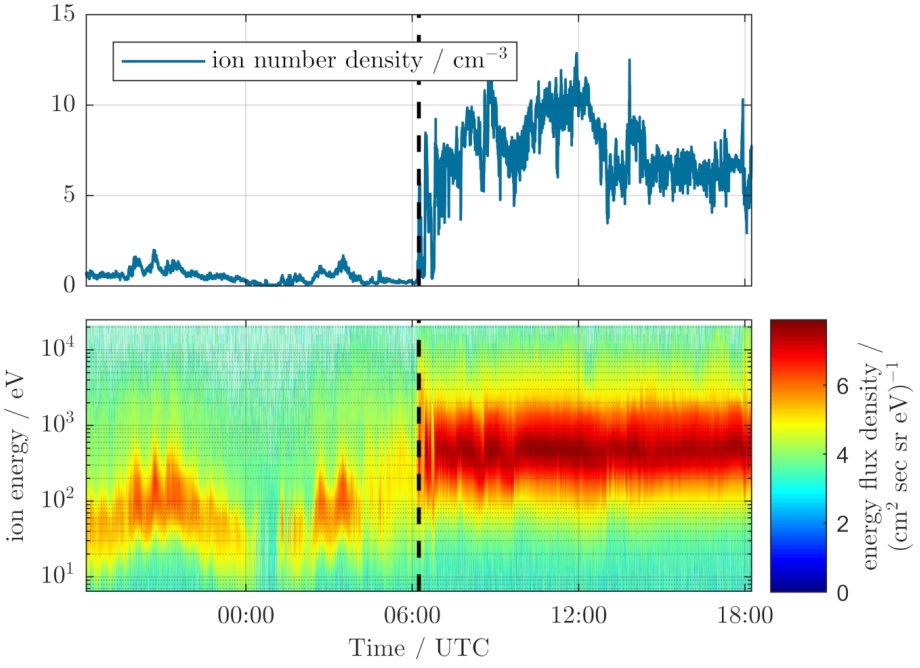

Figure 1. Example for MP crossing of THC on 27 February 2013. The probe comes from the magnetosphere and enters the magnetosheath at around 0614 UTC.

2.3 Identifying MP crossings

Time periods of possible MP crossings are manually selected from the available ESA and FGM data sets when the spacecraft is near, which means about $\pm 10\,\mathrm{R_E}$, the MP position as predicted by the Shue model. The actual crossings are subsequently identified by visual inspection of ESA and FGM measurements. The magnetosheath plasma is characterized by a significant energy flux around 1 keV. This flux almost instantly ceases once the MP has been crossed (Paschmann et al., 1993), see Fig. 1. Furthermore, also the particle number density, as derived from the energy spectrum, exhibits discontinuous changes crossing at the MP. In this way the precise crossing times and conditions are determined. Usually multiple crossings of the MP are also detected during the spacecraft motions into and out of the magnetotail. Contrary to Shue et al. (1997) the outermost crossing is selected for further analysis in the current study. As the outermost crossing we denote the first (last) MP crossing of an inbound (outbound) pass through the boundary region.

A total of 244 transitions is found in this way. For 237 of these SW data are available. Figure 2 displays the spatial distribution of the MP positions determined, projected onto the xy_{GSM}-plane. The figure also shows the expected mean model MP which is acquired by averaging solar wind dynamic pressure and the IMF B_z of all crossing events and using these as the model input parameters. One can easily see that all found MP positions nicely gather around their expected position. Shown as a red dot are the mean positions of each independent point clouds which fall almost exactly onto the model MP.

Ann. Geophys. Discuss., https://doi.org/10.5194/angeo-2018-66
Manuscript under review for journal Ann. Geophys.
Discussion started: 3 July 2018

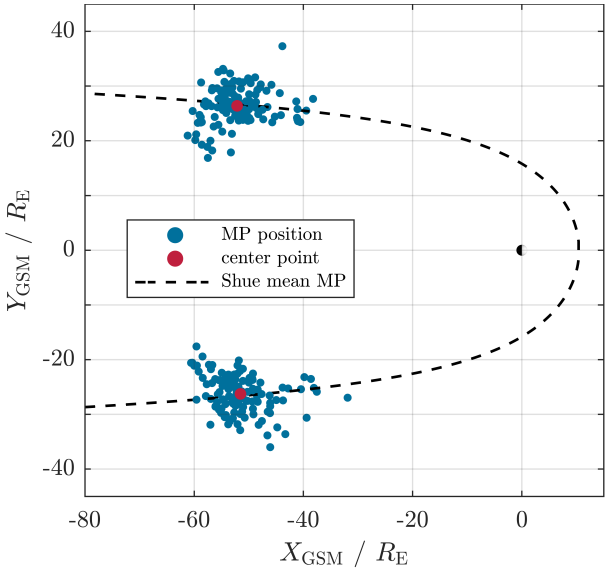

Figure 2. Distribution of MPs projected onto xy_{GSM}-plane. The dashed line shows the mean model magnetopause, for which SW dynamic pressure and magnetic field B_z-component are averaged. The centre points of each independent point cloud is indicated by the red dots.

3 Comparison of position predictions

As the Shue model fits empirical data, fitting parameters for the standoff distance r_0 and the flaring parameter α come with uncertainties (Shue et al., 1997). We interpret this uncertainty as a measure of the standard deviation of the predicted MP position. The resulting MP model range is indicated by the dashed lines in Fig. 3. If any MP distance derived from ARTEMIS observations fall into the thus defined error range δy, see Fig. 3, we regard this MP distance as compatible with the model. We now define the distance between the modelled mean and minimum (maximum) MP distance along the y-axis as the prediction error $\delta y/2$. In a subsequent step the difference Δy between the predicted and actually determined MP, along the y-axis, is normalized to the prediction error $\delta r/2$. Since the magnetopause is almost aligned with the x-axis at lunar distances, no parallax errors need to be taken into account. Using this definition a MP laying exactly at the position predicted by the model has a distance Δy of zero. A MP laying exactly at the model MP with error has the distance Δy of ± 1.

Figure 4 shows the distribution of normalized positions. Approximately $53\,\%$ of the MPs are within the model error as indicated by the vertical dashed dotted red lines. The mean is at $+0.18$ with a standard deviation of 1.56. About $72.2\,\%$ of the data lie within the 1σ-interval and $94.5\,\%$ within the 2σ-interval. The distribution mostly follows a normal distribution and has very similar statistical properties to the Shue model.

The normalized MP distance does not show any strong correlation to the MP position along the x_{GSM}-axis, the strength of the SW B_z-component, or the SW speed. Each of the respective correlation coefficient is below 0.4. As an example, Figure 5 displays the scattering of the x-position against the normalized distance. Because of that, we conclude that there is no systematic deviation between modelled and actually observed MP distance with respect to these parameters.

Ann. Geophys. Discuss., https://doi.org/10.5194/angeo-2018-66
Manuscript under review for journal Ann. Geophys.
Discussion started: 3 July 2018

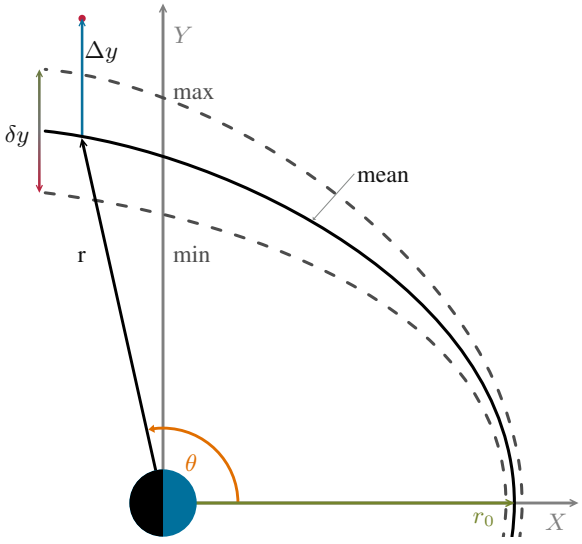

Figure 3. Scheme of the Shue et al. model and the normalization we used. The crossing of the MP with the x-axis is the standoff distance r_0. At certain angle θ the radial distance r of the MP is given. Fitting uncertainties by the model are indicated by the dashed lines. Not shown is the flaring effect α. To characterize the MP position (red dot) the difference distance along the y-axis between model and data, Δy, is normalized by half the error range, δy. (Graphic is not to scale.)

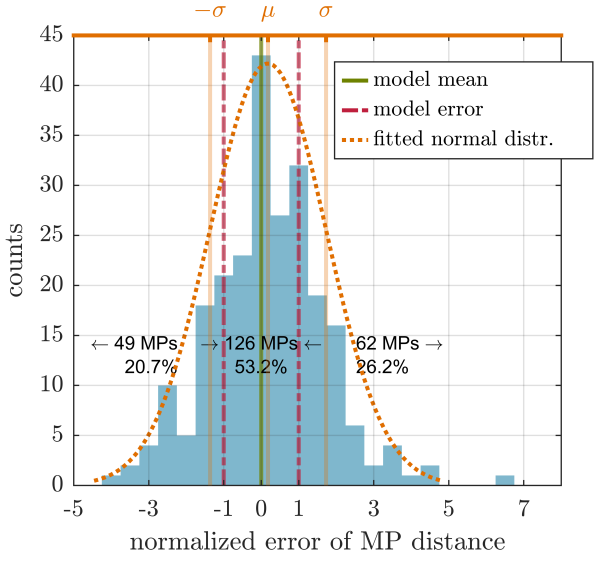

Figure 4. Relative MP position. The error width is indicated by the vertical dashed dotted red line. 53.2 % of MP transitions lay within the model error. The mean is at +0.18, the standard deviation is 1.55. The distribution mostly follows a normal distribution. The skewness of 0.30 and mean indicate a slight tendency of the MP to be found at greater distance to the magnetotail than expected.

Ann. Geophys. Discuss., https://doi.org/10.5194/angeo-2018-66
Manuscript under review for journal Ann. Geophys.
Discussion started: 3 July 2018

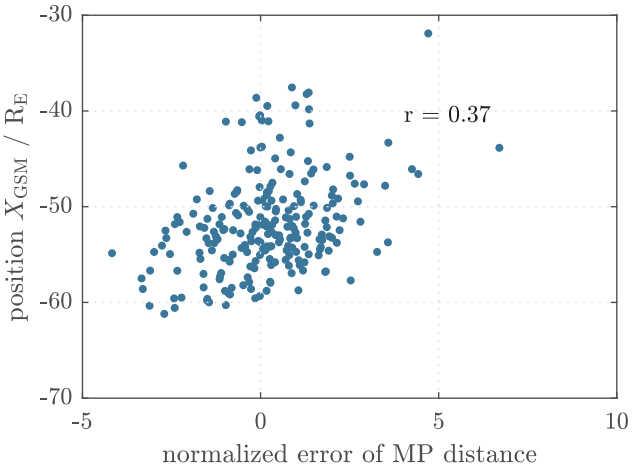

Figure 5. Example for non-existent correlation between the normalized MP distance and the position of the MP projected onto the x_{GSM}-axis. The correlation coefficient is only $r = 0.37$.

4 Comparison of direction predictions

Besides its radial distance, the direction of the magnetopause normal can also be deduced from the Shue model and compared with the observations at lunar distances. For this purpose model and observed normal directions are projected onto the yz-planes (polar plane) and xy-planes (equatorial), respectively, afterwards the deviation angles α, respectively β, between model and observed normal directions are determined. For deviation angles in the yz-plane (xy-plane) the sign of the angle is defined positive for situations in which the actual direction is pointing towards the positive z (x) direction in relation to the model direction. Figure 6 illustrates this angle convention.

The thus defined deviation angles allow to highlight deviations of the magnetopause's opening angle, in case of the angle laying in xy-plane, which corresponds to the Shue flaring parameter, as well as deviations from the ideal axial symmetry, in case of the angle laying in the yz-plane. For each identified crossing solar wind data is used to calculate the model magnetopause. The expected distribution of angles γ between the model normal direction and the y_{GSM}-axis is shown in Fig. 7. Expected are angles with a mean of $5.2\,\mathrm{degrees}$ directed sunwards, or positive direction, following our convention. This reinforces the assumption of negligible parallax errors, see Section 3.

Figures 8 and 9 display the deviation angle distributions. For the xy_{GSM}-plane deviations mean values (median values) of $-2.3\,(0.09)\,\mathrm{degrees}$ for inbound crossings and $6.0\,(8.73)\,\mathrm{degrees}$ for outbound crossings with standard deviations of $29.2\,\mathrm{degrees}$ and $47.2\,\mathrm{degrees}$ are found, respectively. Corresponding values for yz_{GSM}-plane (Figure 8 shows the difference angle between model and data as projected onto the yz_{GSM}-plane are $4.96\,(4.43)\,\mathrm{degrees}$ respective $-5.32\,(-2.95)\,\mathrm{degrees}$ with standard deviations $33.46\,\mathrm{degrees}$ respective $44.66\,\mathrm{degrese}$. The deviation angles exhibit a clear tendency to agglomerate around a vanishing deviation angle. Since we only analysed one crossing event per spacecraft and month as well as the outermost mag-

Ann. Geophys. Discuss., https://doi.org/10.5194/angeo-2018-66
Manuscript under review for journal Ann. Geophys.
Discussion started: 3 July 2018

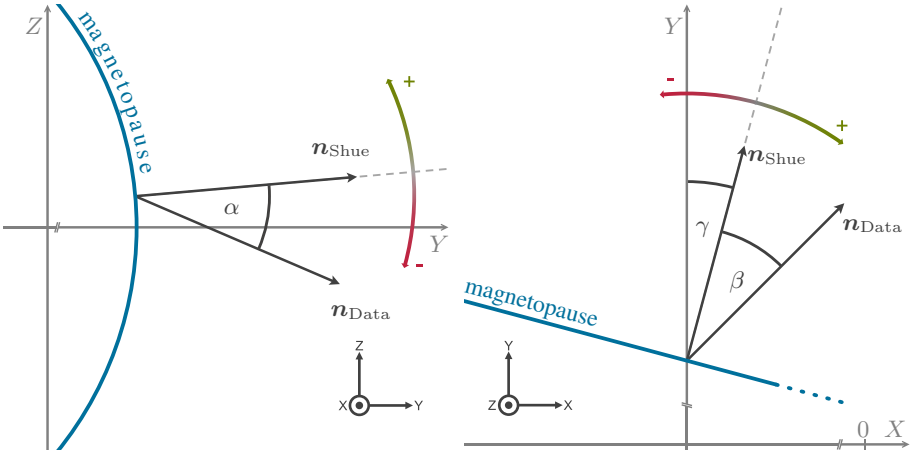

Figure 6. To compare the normal directions of the model and data, angles are measured as deviation from model direction. The angle α (front view, left panel) corresponds to deviation in the rotational symmetry, whereas β (top view, right panel) corresponds to the MP flaring or short term perturbations. The expected opening angle γ of the model is shown in Fig. 7.

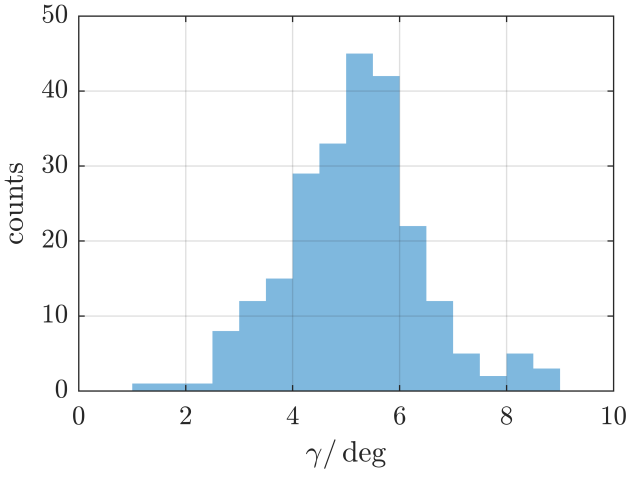

Figure 7. Angle between model MP normal direction of every crossing event and the yz_{GSM}-plane, see angle γ in Fig. 6. Expected are angles with a mean of 5.2 degree.

netopause traversal, the observed scattering is not surprising. We conclude, that predicted normal directions agree well the actual directions, as much as the predicted position does.

Ann. Geophys. Discuss., https://doi.org/10.5194/angeo-2018-66
Manuscript under review for journal Ann. Geophys.
Discussion started: 3 July 2018

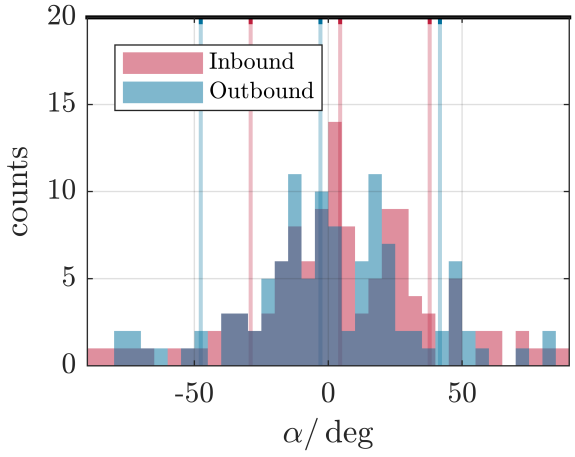

Figure 8. Deviation angle between model and data normal direction as projected onto yz_{GSM}-plane (polar plane). The distribution is separated by inbound (red) and outbound (blue) passes. Indicated by the coloured vertical lines are the respective median angles as well as the standard deviations, see text. The meaning of the angle sign is explained in Fig. 6.

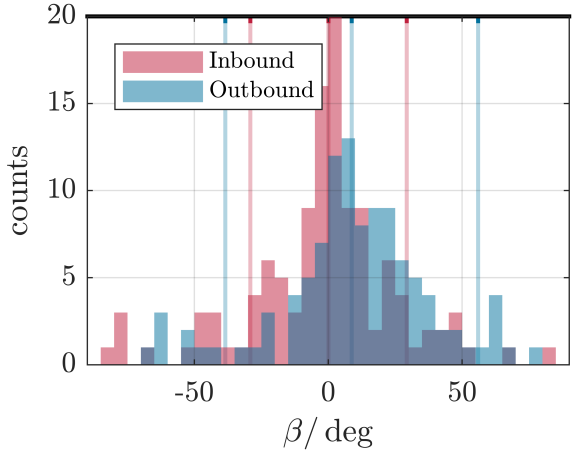

Figure 9. Deviation angle between model and data normal direction as projected onto xy_{GSM}-plane (equatorial plane). The distribution is separated by inbound (red) and outbound (blue) passes. Indicated by the coloured vertical lines are the respective median angles as well as the standard deviations, see text. The meaning of the angle sign is explained in Fig. 6.

Ann. Geophys. Discuss., https://doi.org/10.5194/angeo-2018-66
Manuscript under review for journal Ann. Geophys.
Discussion started: 3 July 2018

Annales Geophysicae Discussions
Open Access
EGU

5 Conclusions

Positions of the magnetopause at lunar distances show very good agreement with those predicted by the Shue model. The distribution of deviations follows a normal distribution with a normalized standard deviation of about 1.5 in units of the model error width and therefore has very similar statistical properties to the Shue model.

The magnetopause normal directions scatter over a wider range of angles, but show a clear tendency to agglomerate around the predicted directions. Since the standard deviation is very large, it is not possible to make a well-founded statement about differences in in- and outbound traversals. Due to the high variability of the magnetopause position caused by constantly changing solar wind conditions, the scattering in normal direction is as expected. Essentially, the axial symmetry of the model can be confirmed for lunar distances in the magnetotail and near to the equatorial plane. Also the flaring parameter of the model fits well into our findings despite high scattering.

On average the Shue model could be validated at lunar distances. We conclude that the model with its consideration of solar wind dynamic pressure and the IMF B_z component most adequately describes the behaviour of magnetopause. Even for the mid-magnetotail these two parameters are the most important drivers for magnetopause movement.

Data availability. THEMIS data and the latest calibration files are publicly available at http://themis.ssl.berkeley.edu/ or via the SPEDAS software.

Competing interests. The authors declare that they have no conflict of interest.

Acknowledgements. We acknowledge use of NASA/GSFC's Space Physics Data Facility's OMNIWeb service, and OMNI data. We acknowledge NASA contract NAS5-02099 and V. Angelopoulos for use of data from the THEMIS Mission - specifically, C. W. Carlson and J. P. McFadden for use of ESA data. This study is financially supported by the German Ministerium für Wirtschaft und Energie and the Deutsches Zentrum für Luft- und Raumfahrt under contract 50 OC 1403.

References

Angelopoulos, V.: The THEMIS Mission, Space Science Reviews, 141, 5–34, https://doi.org/10.1007/s11214-008-9336-1, 2008.

Angelopoulos, V.: The ARTEMIS Mission, Space Science Reviews, 165, 3–25, https://doi.org/10.1007/978-1-4614-9554-3_2, 2010.

Auster, H. U., Glassmeier, K. H., Magnes, W., Aydogar, O., Baumjohann, W., Constantinescu, D., Fischer, D., Fornacon, K. H., Georgescu, E., Harvey, P., Hillenmaier, O., Kroth, R., Ludlam, M., Narita, Y., Nakamura, R., Okrafka, K., Plaschke, F., Richter, I., Schwarzl, H., Stoll, B., Valavanoglou, A., and Wiedemann, M.: The THEMIS Fluxgate Magnetometer, Space Science Reviews, 141, 235–264, https://doi.org/10.1007/s11214-008-9365-9, https://doi.org/10.1007/s11214-008-9365-9, 2008.

Glassmeier, K.-H., Auster, H.-U., Constantinescu, D., Fornaçon, K.-H., Narita, Y., Plaschke, F., Angelopoulos, V., Georgescu, E., Baumjohann, W., Magnes, W., Nakamura, R., Carlson, C. W., Frey, S., McFadden, J. P., Phan, T., Mann, I., Rae, I. J., and Vogt, J.: Magnetospheric quasi-static response to the dynamic magnetosheath: A THEMIS case study, Geophysical Research Letters, 35, https://doi.org/10.1029/2008gl033469, 2008.

Hansen, K. C., Bagdonat, T., Motschmann, U., Alexander, C., Combi, M. R., Cravens, T. E., Gombosi, T. I., Jia, Y.-D., and Robertson, I. P.: The Plasma Environment of Comet 67P/Churyumov-Gerasimenko Throughout the Rosetta Main Mission, Space Science Reviews, 128, 133–166, https://doi.org/10.1007/s11214-006-9142-6, 2007.

Hapgood, M.: Space physics coordinate transformations: A user guide, Planetary and Space Science, 40, 711–717, https://doi.org/10.1016/0032-0633(92)90012-d, 1992.

Lin, R. L., Zhang, X. X., Liu, S. Q., Wang, Y. L., and Gong, J. C.: A three-dimensional asymmetric magnetopause model, Journal of Geophysical Research: Space Physics, 115, https://doi.org/10.1029/2009JA014235, 2010.

McFadden, J. P., Carlson, C. W., Larson, D., Ludlam, M., Abiad, R., Elliott, B., Turin, P., Marckwordt, M., and Angelopoulos, V.: The THEMIS ESA Plasma Instrument and In-flight Calibration, Space Science Reviews, 141, 277–302, https://doi.org/10.1007/s11214-008-9440-2, 2008.

Paschmann, G. and Daly, P. W.: Analysis Methods for Multi-Spacecraft Data, ESA Publications Division, 1998.

Paschmann, G., Baumjohann, W., Sckopke, N., Phan, T. D., and Lühr, H.: Structure of the dayside magnetopause for low magnetic shear, Journal of Geophysical Research: Space Physics, 98, 13 409–13 422, https://doi.org/10.1029/93ja00646, 1993.

Shue, J.-H. and Song, P.: The location and shape of the magnetopause, Planetary and Space Science, 50, 549–558, https://doi.org/10.1016/S0032-0633(02)00034-X, 2002.

Shue, J.-H., Chao, J. K., Fu, H. C., Russell, C. T., Song, P., Khurana, K. K., and Singer, H. J.: A new functional form to study the solar wind control of the magnetopause size and shape, Journal of Geophysical Research: Space Physics, 102, 9497–9511, https://doi.org/10.1029/97ja00196, 1997.

Wang, Y., Sibeck, D. G., Merka, J., Boardsen, S. A., Karimabadi, H., Sipes, T. B., Šafránková, J., Jelínek, K., and Lin, R.: A new three-dimensional magnetopause model with a support vector regression machine and a large database of multiple spacecraft observations, Journal of Geophysical Research: Space Physics, 118, 2173–2184, https://doi.org/10.1002/jgra.50226, 2013.